Journal Pre-proof

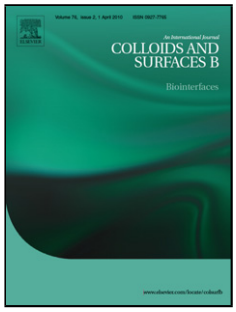

Immobilization of fenugreek β-amylase onto functionalized tungsten disulfide nanoparticles using response surface methodology: its characterization and interaction with maltose and sucrose

Dinesh Chand Agrawal, Anjali Yadav, Vijay K. Singh, Anchal Srivastava, Arvind M. Kayastha

PII: S0927-7765(19)30744-1

DOI: https://doi.org/10.1016/j.colsurfb.2019.110600

Reference: COLSUB 110600

To appear in: *Colloids and Surfaces B: Biointerfaces*

Received Date: 10 July 2019

Revised Date: 20 September 2019

Accepted Date: 17 October 2019

Please cite this article as: Agrawal DC, Yadav A, Singh VK, Srivastava A, Kayastha AM, Immobilization of fenugreek β-amylase onto functionalized tungsten disulfide nanoparticles using response surface methodology: its characterization and interaction with maltose and sucrose, *Colloids and Surfaces B: Biointerfaces* (2019), doi: https://doi.org/10.1016/j.colsurfb.2019.110600

Immobilization of fenugreek *β*-amylase onto functionalized tungsten disulfide nanoparticles using response surface methodology: its characterization and interaction with maltose and sucrose

Dinesh Chand Agrawal[a], Anjali Yadav[a], Vijay K Singh[b], Anchal Srivastava[b] and Arvind M. Kayastha[a]*

[a]School of Biotechnology, Institute of Science, Banaras Hindu University, Varanasi 221005, India

[b]Department of Physics, Institute of Science, Banaras Hindu University, Varanasi 221005, India

***Corresponding author:** Arvind M. Kayastha

E-mail address: kayasthabhu@gmail.com

Tel.: +91 542 2368331

Fax: +91 542 2368693

Graphical Abstract

Schematic representation of immobilization process

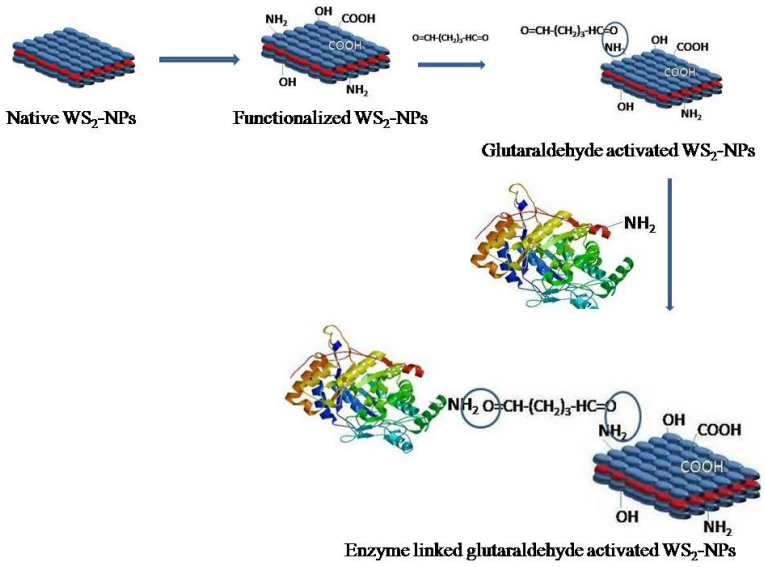

Highlights

- *β*-Amylase was immobilized on WS_2-NPs.
- Immobilization was confirmed by SEM, FT-IR, AFM and Fluorescence microscopy.
- Maltose and sucrose fluorescence biosensors were prepared.
- The process was spontaneous and endothermic, driven by hydrophobic interactions

Abstract

In this communication, fenugreek *β*-amylase was immobilized onto functionalized tungsten disulfide nanoparticles through cross-linker glutaraldehyde and successful immobilization was confirmed by SEM, AFM and FTIR spectroscopy. To make the process economical and efficient, optimization of independent variables was carried out using Box-Behnken design of response surface methodology. Approximately similar predicted (85.6%) and experimental (84.2%) immobilization efficiency revealed that the model is suitable for design of space. Optimum temperature was calculated to be 60 ºC. After immobilization, an increased K_m (2.12 times) and a decreased V_{max} (0.58 times), indicated inaccessibility of active site residues to the substrate. The immobilized enzyme retained 77% relative activity after 10 uses whereas 40%

residual activity was obtained after 120 days. An increased half-life with concomitantly decreased kinetic rate constant revealed that the immobilized enzyme is more stable at a higher temperature and the process followed first-order kinetics ($R^2 > 0.93$). The limit of detection for maltose and sucrose fluorescence biosensor was found to be 0.052 and 0.096 mM, respectively. Thermodynamic parameters such as changes in Gibbs free energy ($\Delta G < 0$), enthalpy ($\Delta H > 0$) and entropy ($\Delta S > 0$) revealed that the process is spontaneous and endothermic, driven by hydrophobic interactions. Thermo-stability data at higher temperature for the immobilized enzyme makes it a suitable candidate for industrial applications in the production of maltose in food and pharmaceutical industries. Furthermore, fluorescence biosensor could be used to detect and quantify maltose and sucrose to maintain the quality of industrial products.

Keywords: *β*-Amylase; Tungsten disulfide; Immobilization; Thermodynamic parameters; Fenugreek

Introduction

β-Amylase (malto-hydrolase) is a non-metallo maltogenic enzyme, which hydrolyzes starch and related polysaccharides, by cleaving *α*-1,4 linkage from the non-reducing end and releases *β*-maltose along with traces amount of *β*-limit dextrin [1-3]. Maltose is used for the production of maltose rich syrup, artificial sweeteners, bread and wine [4]. Moreover, it has also been proved in human that mutant of *SI* gene is responsible for congenital sucrase-isomaltase disorder, which affects the digestion of sucrose and maltose and might require the elimination of these sugars from the diet [5]. Therefore, for consumer protection, actual measurement of sugar content becomes an important criterion in the agriculture and food processing industries. Different techniques such as nuclear magnetic resonance, circular dichroism and electron spin resonance have been employed for measuring sugar contents and binding constants of ligands with macromolecules [6]. Fluorescence spectrometry is an efficient, highly sensitive and simple tool for determining these sugar contents by measuring fluorescence intensity and thermodynamic parameters of ligand-macromolecule interactions [7, 8]. However, the use of the enzyme in

water-soluble form has some limitations such as lack of thermal stability, long term storage stability, sensitivity to change in pH, temperature and difficult to recover, which make the enzyme to be unsuitable for industrial applications. These drawbacks can be overcome by immobilizing the enzyme on water-insoluble matrix using a suitable method [9-12]. Various methods such as adsorption [13, 14], entrapment [15, 16], affinity [17, 18] and covalent binding [9, 10, 19, 20] have been used for immobilization of enzymes. Covalent binding using a cross-linker prevent leakage of the enzyme and stabilizes the binding protein thereby increases immobilization efficiency [10, 20]. Immobilization efficiency is also affected by supporting materials. Therefore, the present requirement is to explore and utilize novel materials to maximize optimum interaction between support and enzyme for achieving better immobilization efficiency along with high stability and reusability [21]. Due to unique characteristics such as non-toxic nature and greater thermal stability, carbon derived materials such as graphene and its derivatives have acquired tremendous consideration in biotechnology applications [22, 23]. However, due to lack of functionalities, heavy acid treatment for activation, poor thermal and electrical conductivity limit the use of these materials for sensing purposes [19, 24].

Nowadays, due to high specific surface area and ideal electronic structure transition metal dichalcogenides (TMDs) such as molybdenum disulfide (MoS_2) and tungsten disulfide (WS_2) are being used as matrix of enzyme immobilization for biosensor construction. WS_2 has a layered structure, which is connected by Van der Waals' interactions. Like MoS_2 one tungsten layer sandwiched between two layers of sulfur, which resist agglomeration that makes them a suitable material for enzyme immobilization [25, 26].

Enzyme immobilization efficiency decides the cost of an industrial product, which depends on process parameters. That is why; process optimization becomes an important step for any industrial process. Different approaches of process optimization such as Taguchi, Factorial and Response Surface Methodology (RSM) have been applied, among them; RSM is robust, cost-effective as well as time-saving method. RSM uses different statistical methods and suggests single optimum model using analysis of variance. Subsequently, to get more information about interactions and response the model is visualized by 2-D contour and 3-D response plots [19, 27, 28].

This communication includes immobilization of purified fenugreek β-amylase [29] onto glutaraldehyde activated WS_2-NPs. To optimize process parameters Box-Behnken design of RSM was employed. The immobilized enzyme was characterized using SEM, AFM, FTIR, confocal and fluorescence microscopy. Finally, the immobilized enzyme was used to construct fluorescence biosensor to detect maltose and sucrose and subsequently thermodynamic as well as kinetic parameters were calculated to find out the nature of interaction between immobilized fenugreek β-amylase and sugar molecule.

Materials and methods

Chemicals

Sodium tungstate dihydrate ($Na_2WO_4.2H_2O$), NaCl and HCl were procured from Hi-Media chemicals, India. Elemental sulfur was procured from Alfa Aesar, India. Glutaraldehyde, 3,5-dinitrosalicylic acid (DNS), soluble starch, fluorescein isothiocyanate (FITC) and bovine serum albumin (BSA) were acquired from Sigma-Aldrich, St. St. Louis, MO. All the chemicals for preparation of buffers were analytical grade and purchased from SISCO (Sisco Research Laboratories Pvt. Ltd.) India. Milli-Q (MQ) quality water was used throughout all experiments having the resistance higher than 18 MΩ.cm (Millipore, Bedford, MA, USA).

Synthesis of WS_2-NPs

WS_2-NPs were synthesized following the two step synthesis process. During first step, tungsten oxide nanorods were synthesized using hydrothermal approach reported previously by our group [30]. In the second step, WO_3 was sulfurized in high temperature furnace at ~1000 ºC in presence of inert Ar gas and ambience of sulfur for obtaining WS_2-NPs.

Enzyme preparation

The enzyme was purified from fenugreek seeds using acetone fraction (45-60 %), ion-exchange chromatography on CM-cellulose and glycogen affinity precipitation. The purified enzyme has specific activity of 833.3 μmol/min/mg of protein and homogeneity was confirmed by SDS-PAGE [29].

Immobilization of fenugreek *β*-amylase onto functionalized WS_2-NPs

A suspension of WS_2-NPs (1 mg/mL) was prepared in 50 mM Tris-HCl buffer (pH 7.5) followed by sonication for 2 h. Thereafter, based on Box-Behnken design, the suspension was distributed into 29 runs as shown in **Table 1.** After that, all the samples were equilibrated overnight in the same buffer and then treated with glutaraldehyde for 4 h in dark at room temperature. Subsequently, the aliquots were washed (thrice) to remove unbound glutaraldehyde followed by overnight incubation with the enzyme at 4 °C. Immobilized enzyme was obtained by centrifugation of the aliquots at 5000 rpm for 2 min and stored in the same buffer at 4 °C [19].

Table 1: Box-Behnken design showing independent variables and corresponding actual and predicted % immobilization at three factor levels

Run	pH	Glutaraldehyde (%; v/v)	Enzyme (µg)	Tungsten disulfide (µg)	Immobilization	
					Actual (%)	Predicted (%)
1	7.5	3	200	750	55.34	56.17
2	6.5	2	100	750	54.57	53.17
3	6.5	2	150	500	52.68	52.88
4	7.5	2	200	1000	55.45	54.81
5	6.5	2	150	1000	54.56	54.22
6	7.5	1	150	1000	52.67	54.57
7	7.5	2	150	750	83.67	85.56
8	7.5	2	150	750	85.78	85.56
9	7.5	2	100	500	52.45	53.82
10	7.5	3	150	500	57.67	55.39
11	8.5	2	150	500	52.45	52.41
12	7.5	1	200	750	54.67	52.94

13	8.5	1	150	750	51.56	51.55
14	8.5	2	150	1000	51.67	51.09
15	7.5	2	200	500	53.45	54.41
16	6.5	2	200	750	55.67	55.20
17	6.5	3	150	750	53.45	54.19
18	7.5	3	100	750	51.45	52.80
19	7.5	2	100	1000	53.67	53.44
20	7.5	2	150	750	87.92	85.56
21	8.5	2	100	750	52.34	52.43
22	7.5	2	150	750	85.67	85.56
23	7.5	2	150	750	84.78	85.56
24	7.5	3	150	1000	52.45	52.30
25	6.5	1	150	750	51.56	52.80
26	7.5	1	100	750	55.56	54.35
27	7.5	1	150	500	51.67	51.44
28	8.5	2	200	750	51.34	52.36
29	8.5	3	150	750	52.34	51.83

Protein assay

Protein amount was assayed by the modified method of Lowry [31], and bound protein was measured by the following expression:

$$\text{Bound protein (mg)} = \text{loaded protein (mg)} - \text{protein present in washing solution (mg)}.$$

Determination of fenugreek *β*-amylase activity (EC: 3.2.1.2)

The activity of the soluble and immobilized enzyme was measured by the method of Bernfeld [32].

Determination of soluble fenugreek *β*-amylase activity

To measure *β*-amylase activity, 0.5 mL diluted enzyme was added to 0.5 mL (1%) soluble starch followed by 3 min incubation at room temperature. Thereafter, 1 mL of DNS was added followed by 5 min incubation in a boiling water bath. Subsequently, 10 mL MQ water was added

and absorbance was recorded at 540 nm using JASCO V-630 uv/vis spectrophotometer (JASCO Corporation, Hachioji-shi, Tokyo, Japan) [29, 32].

Determination of immobilized fenugreek *β*-amylase activity

A reaction mixture was prepared by mixing the immobilized enzyme with 0.5 mL of substrate at room temperature for 3 min and subsequently, centrifugation was carried out at 5000 rpm for 2 min. Supernatant was collected and activity was measured as soluble enzyme.

Immobilization efficiency

$$\text{Immobilization efficiency} = \frac{\text{Specific activity of immobilized } \beta\text{-amylase}}{\text{Specific activity of soluble } \beta\text{-amylase}} \times 100$$

Process optimization using Response Surface Methodology

Before applying the Box-Behnken design of RSM, it is prerequisite to perform preliminary experiments to find out higher and lower values of independent variables. Therefore, in our work four variables as given in **Table 1** were used to optimize the response (immobilization efficiency) and preliminary experiments were conducted. The data thus obtained for higher and lower values were entered to Design expert software, which generates 29 sets of experiments as shown in **Table 1**. To validate the sets, experiments were conducted in all conditions (**Table 1**) and regression analysis was carried out to study the relationship between independent variables and response using second order polynomial equation [33] as shown below:

$$Y = B_0 + \sum B_i X_i + \sum B_{ii} X_i^2 + \sum B_{ij} X_i X_j$$

where, Y represents a predicted response variable or independent variable

X_i and X_j represent input independent variables which influence response variable Y

B_o represents the offset term; B_i represents the i^{th} linear coefficient

B_{ii} represents the i^{th} quadratic coefficient

B_{ij} represents the ij^{th} interaction coefficient

Satisfactoriness of accepting the model was tested by comparing parameters such as lack-of-fit p-value, sequential p-value, predicted R^2 and adjusted R^2 values [34, 35]. Furthermore, interaction among different factors and response was studied using 2-D contour and 3-D plots [33].

Characterization of immobilized *β*-amylase

Scanning Electron Microscope

In this communication SEM (Philips: XL20) was used to characterize the surface morphology of WS_2-NPs. Native, glutaraldehyde-activated and enzyme-linked WS_2-NPs were air-dried (20 μL) and placed on a metallic (silver) stub using adhesive and then transferred to the machine, subsequently, images were recorded at different magnification powers.

Fourier Transform Infrared Spectroscopy

FTIR spectrum is used to identify types of chemical bonds and the functional groups present in a molecule based on their vibrational frequencies [36]. Average of 250 spectra was taken as resultant spectrum to find out the relationship between infrared frequency peaks and molecular structure in the scan range 400 – 4000 cm^{-1} using Perkin Elmer (Spectrum 100, USA) spectrometer.

Fluorescence and Confocal Laser Scanning Microscopy

Fluorescence (Nikon DS-Fi1) and confocal laser scanning microscope (Carl Zeiss 800) were used to analyze micrographs using the fluorescence signals, generated by FITC tagged fenugreek *β*-amylase after immobilization onto WS_2-NPs. *β*-Amylase coupled WS_2-NPs and bare WS_2-NPs were stained with 100 μL FITC solution (1 mg/mL) prepared in dimethylformamide (DMF), followed by incubation in dark at 4 °C for 1 h. Subsequently, unlabeled FITC was removed by washing (twice) with MQ water and samples were analyzed using fluorescence and confocal microscope at 10X and 20X magnification powers, respectively [19].

Atomic Force Microscope

To deduce the surface topography of enzyme-linked WS_2-NPs and native WS_2-NPs at single-molecule level with sub-nanometer accuracy, AFM (NT-MDT Russia, NTEGRA PRIMA model) analysis was carried out [37]. 20 μL of native WS_2-NPs (750 μg/mL) and 20 μL enzyme cross-linked WS_2-NPs (0.15 mg/mL) were placed on cleaned glass slides and air-dried followed by image acquisition and statistical (Roughness average and Root mean square roughness) analysis.

Kinetic studies

The amount of soluble (150 μg) and immobilized (200 μg/mg of the matrix) fenugreek β-amylase was kept constant as determined by the RSM. Each experiment was performed three times and standard deviation was expressed as error bar using Sigma plot version 8.0.

Effect of pH

The optimum pH of fenugreek β-amylase (soluble and immobilized) was determined by preparing the soluble starch in Glycine-HCl (pH 2.0-3.0), Sodium-acetate (pH 4.0-5.0), Sodium-phosphate (pH 6.0-7.0), Tris-HCl (pH 7.2-9.0) and Glycine-NaOH (pH 9.0-11.0) buffers of 0.050 M [29] followed by measuring the activity according to the procedure described in the above section.

Effect of temperature

To find out optimum temperature of germinated fenugreek β-amylase (both soluble and immobilized) activity with respect to soluble starch as substrate was determined in the temperatures range of 30 to 90± 1°C (water bath; Pharmacia multitemp II) according the procedure described in the above section.

Effect of substrate concentration

To determine the effect of substrate concentration, activity of the enzyme with respect to varying concentrations (1.0–10 mg/mL) of starch were calculated according the procedure described in the above section and data thus obtained for both enzymes (soluble and immobilized) were fitted to Lineweaver-Burk plot and using x and y-intercept K_m and V_{max} were calculate.

Storage stability

Storage stability was investigated by determining residual activity (%) of free and enzyme-linked WS_2-NPs for 120 days at 4 ºC at regular time interval using the procedure described in the above section. The activity of first time was considered as 100% [9].

Reusability

0.5 mL (1%) soluble starch was prepared in 50 mM sodium phosphate buffer (pH 6.5) and added to enzyme coupled WS_2-NPs followed by 3 min incubation at 30 ºC. At the end of the assay reaction, supernatant was collected in a separate glass tube and assayed for disaccharide β-maltose using DNS method. Enzyme coupled WS_2-NPs were washed twice using MQ water and then substrate solution was added to start a new cycle.

Thermal stability

Thermal inactivation study was carried out by incubating the enzyme (both) at different temperature ranging from 30-70 °C for different time interval. After incubation time, the mixture was cooled down at room temperature and residual activity was recorded using the procedure described in the above section. Initial activity was considered as 100%. A plot was drawn between $\ln(v/v_o)$ and time interval (t) at each temperature and kinetic rate constant (k) as well as half life ($t_{1/2}$) were calculated using following expressions.

$$\ln \frac{v}{v_o} = k \, .t \quad \text{---------- (1)}$$

$$t_{1/2} = \frac{0.693}{k} \quad \text{---------- (2)}$$

where, v_o is initial activity and v is residual enzymatic activity at time t [38].

Interaction of sugars with *β*-amylase

The tryptophan fluorescence of *β*-amylase

To study the effect of maltose (1-4 mM) and sucrose (1-5 mM) on the fluorescence power of tryptophan residues, fenugreek *β*-amylase (0.15 mg/mL) was prepared in sodium-phosphate buffer (pH 6.5) at 30 ºC. The enzyme was then excited at a wavelength of 295 nm and emission spectra were recorded in the range of 320 to 370 nm using spectrofluorometer (Cary Eclipse; Varian).

Stern-Volmer plot and limit of detection (LOD)

Stern-Volmer plot was used to find out the linear relationship between changes in the fluorescence intensity (F_0/F_x) with respect to concentrations of sugars using the following relationship [6]

$$\frac{F_0}{F_x} = 1 + K_{sv}[Q] \quad \text{.....(1)}$$

where, F_x and F_0 are fluorescence intensities of the immobilized enzyme in the presence and absence of sugars, respectively. [Q] is concentration of sugar, K_{SV} is the Stern–Volmer quenching constant.

Quenching plot was drawn between fluorescence intensity and concentration of ligand, which was used to calculate limit of detection (LOD) using the following relationship:

$$LOD = \frac{3\eta}{m} \quad \text{.....(2)}$$

where, η is the standard deviation of blank and m is the slope of the quenching graph.

Determination of dissociation constant (K_d) and thermodynamic parameters

Sugar solution of maltose (1mM) and immobilized enzyme were kept at 30 ºC in a temperature controlled water bath (Pharmacia MultiTemp II) for 5 min. Later, the enzyme and sugar solution were mixed in a cuvette and subsequently, spectra were recorded at the same temperature. Similar procedure was carried out for varying concentrations of maltose and sucrose at 30 ºC and

40 ºC. The data thus obtained were fitted to Hanes-Woolf plot to calculate the value of dissociation constant [39] using following expressions:

$$\frac{[Q]}{\Delta F} = \frac{K_d}{\Delta F_{max}} + \frac{[Q]}{\Delta F_{max}} \quad \text{..... (3)}$$

where, ΔF is the difference between fluorescence intensity in the absence and presence of ligand whereas ΔF_{max} is fluorescence intensity in the absence of ligand minus maximum decrement in the fluoresce intensity in the presence of the ligand.

The changes in the enthalpy (ΔHº) of maltose and sucrose were determined using the following van't Hoff equation [40].

$$\ln K_d = (\Delta H^o / R)\,(1/T) - \Delta S^o / R \quad \text{……..(4)}$$

The changes in Gibbs free energy (ΔGº) and entropy (ΔSº) were calculated from equations 5 and 6 [6].

$$\Delta G^o = -RT \ln K_d \quad \text{……..(5)}$$

$$T\Delta S^o = \Delta H^o - \Delta G^o \quad \text{…….(6)}$$

where, R is the universal gas constant (8.31 J/mol/K) and T is the absolute temperature in Kelvin.

Results and discussions

Synthesis of WS_2-NPs:

The morphology of as synthesized WS_2 was characterized using Scanning electron microscope **(Fig. 1a).** Here we can clearly see the nanoparticles of WS_2 in the range of ~ 200 nm. Further, in order to unveil the crystal structure of WS_2-NPs, X-ray diffraction at room temperature was recorded using Cu Kα (λ~ 1.54 Å) radiation and shown in **Fig. 1(c)**. All of the peaks are indexed and matched well with the hexagonal phase of WS_2 structure (JCPDS Card Number: 84-1398). We have also recorded the Raman spectrum (**Fig. 1b**) for confirming the presence of WS_2-NPs. Two main characteristic peaks at ~349 cm^{-1} and ~418 cm^{-1} are observed, which are known as

E_{2g}^1 and $A_{1}g$ modes and corresponded to the 'in plane' and 'out of plane' vibrations of tungsten (W) and sulfur (S) atoms, respectively. Further, the separation between E_{2g}^1 and $A_{1}g$ modes $\Delta\nu$ ~69 cm^{-1} between E_{2g}^1 and A_{1g} modes corresponds to the multilayer nature of WS_2-NPs.

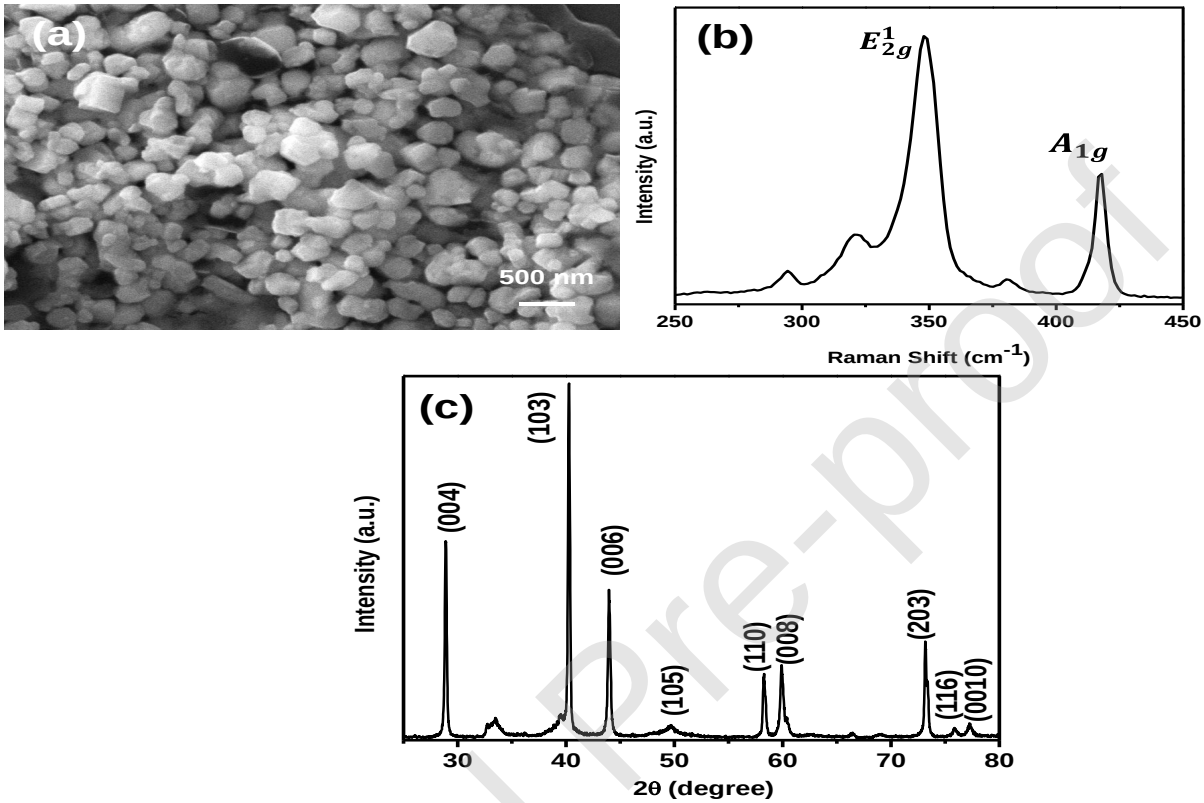

Fig. 1: (a) SEM image **(b)** Raman spectrum **(c)** XRD pattern of WS_2-NPs confirming the presence of hexagonal phase of WS_2.

Optimization of purified fenugreek *β*-amylase using RSM

To achieve maximum immobilization efficiency, it is a pre-requisite that an enzyme should be attached to a suitable matrix with proper orientation and configuration [41]. Subsequently, kinetics and thermodynamic parameters should be optimized to decrease the operational cost of an industrial process [42, 43]. In this communication, to achieve the goal of maximum immobilization efficiency statistical approaches were used for understanding the relationship between process parameters (variables) and response of the immobilized enzyme. Interactions of four variables at three different levels and their effects on the response were studied using RSM and results are shown in **Table 1**. Data thus obtained were fitted to generate different models

(**Table 2A**) and based on sequential p-value, lack of fit p-value, adjusted R^2 and predicted R^2 [34, 35] quadratic model was suggested (**Table 2A).**

Table 2 (A): Different models based on Analysis of Variance

Source	**Sequential p-value**	**Lack of Fit p-value**	**Adjusted R^2**	**Predicted R^2**	
Linear	0.9991	0.0003	-0.1627	-0.1588	
2FI	1.0000	0.0001	-0.5437	-0.4625	
Quadratic	**< 0.0001**	**0.5379**	**0.9840**	**0.9634**	**Suggested**
Cubic	0.3097	0.7328	0.9878	0.9421	Aliased

(B): Analysis of variance for quadratic model generated using Box-Behnken design

Source	**Sum of Squares**	**Df**	**Mean Square**	**F-value**	**p-value**	**(Prob>F)**
Model	4332.98	14	309.50	124.12	<0.0001	Significant
Residual	34.91	14	2.49			
Lack of Fit	25.10	10	2.51	1.02	0.5379	Not significant

Pure Error	9.81	4	2.45

Predicted R^2 and Adjusted R^2 values were found to be 0.96 and 0.98, respectively. The difference between the values is lesser than 0.2, which revealed the model is well-fitted for experimental design space. To fit the model, the lack of fit p-value should be insignificant with respect to pure error. The data presented in **Table 2B** reveals that lack of fit p-value is insignificance, which supports the model to be significant for design of experiment. Multiple correlation coefficient (R^2) value was found to be 0.99, which revealed good relationship between predicted and actual immobilization efficiency as shown in **Fig 2C** [33]. After the model was suggested, regression analysis was carried out and final equation is shown below:

$$\textbf{Immobilization (\%)} = +85.56 - 0.8992 \times A + 0.4175 \times B + 0.4900 \times C - 0.0083 \times D - 0.2775 \times A \times B - 0.5250 \times A \times C - 0.6650 \times A \times D + 1.20 \times B \times C - 1.55 \times B \times D + 0.1950 \times C \times D - 16.87 \times A^2 - 16.10 \times B^2 - 15.40 \times C^2 - 16.04 \times D^2$$

where A, pH; B, Glutaraldehyde concentration (%; v/v); C, Enzyme (μg); D, WS_2-NPs (μg).

To acquire better understanding of the results, graphical analysis was carried out using 3-D response surface and contour plots [33], which revealed the mutual effect of variables on immobilization efficiency as shown in **Fig. 2A, 2B**.

Under optimum conditions (**Fig. 2)** predicted maximum immobilization efficiency (85.58%) was very close to actual (84.21%), which revealed success of immobilization. Similar results were obtained by other researchers [19, 36].

(A)

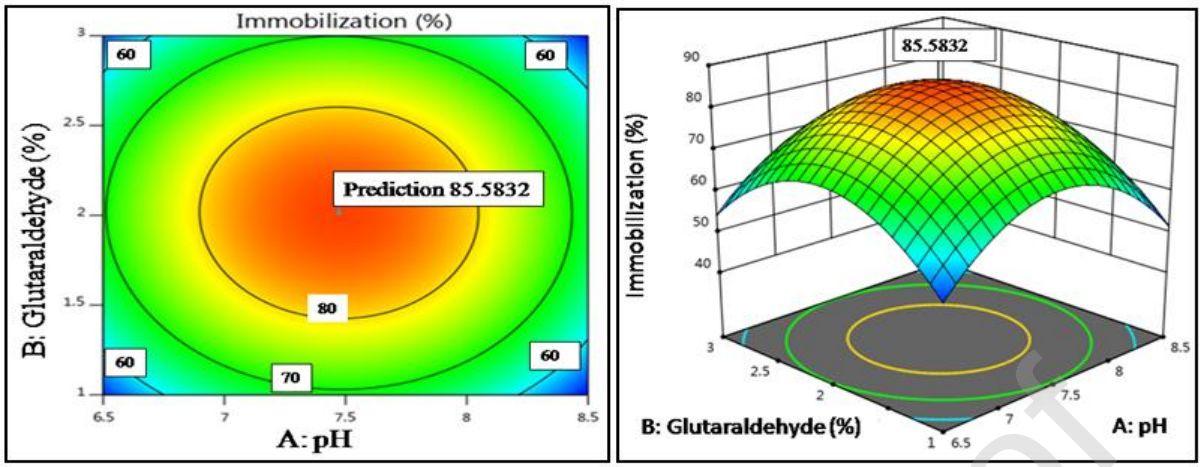

(B)

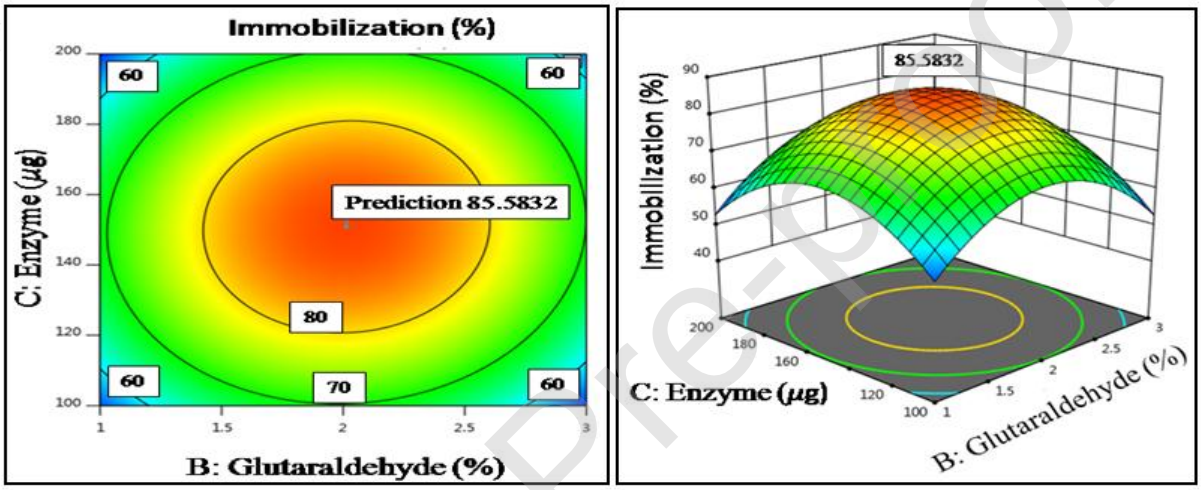

Optimum conditions

WS_2-NPs	: 750 μg
pH	: 7.43
Glutaraldehyde	: 2.01%
Protein	: 150.84 μg
Predicted	: 85.58%
Experimental	: 84.21%

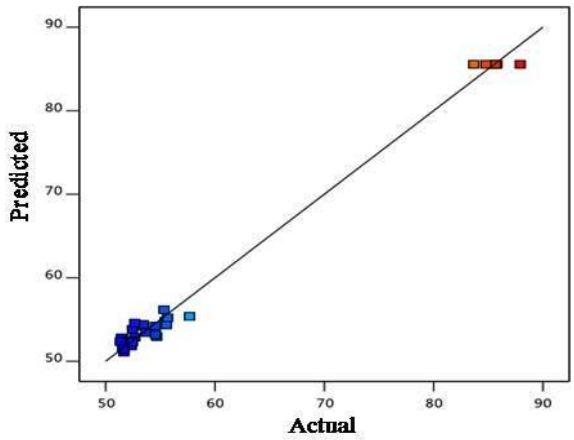

(C)

Fig. 2: 2-D contour and corresponding 3-D plots of *β*-amylase showing the effects of **(A)** glutaraldehyde and pH **(B)** glutaraldehyde and enzyme on % immobilization **(C)** linear relationship between actual and predicted immobilization efficiency.

Characterization of immobilized *β*-amylase

To confirm the immobilization of *β*-amylase onto WS_2-NPs, SEM**,** AFM, FTIR and Fluorescence and Laser Scanning Confocal Microscopy were employed.

Scanning Electron Microscopy

It has been proved that attachment of an enzyme onto a matrix results, changes in surface morphology of matrix, which reveal the successfulness of the immobilization process [10, 44]. The study of surface morphology of native WS_2-NPs **(Fig. Sa)**, glutaraldehyde-activated WS_2-NPs **(Fig. Sb)** and enzyme-linked WS_2-NPs **(Fig. Sc)** using SEM revealed successful immobilization of the enzyme onto WS_2-NPs.

Fourier Transform Infrared Spectroscopy

For further confirmation of the immobilization, FTIR analysis was performed, which generates a specific vibrational frequency for each chemical bond that works as a molecular fingerprint, which provide the information about the nature of bonds and molecules. FTIR spectrum obtained for functionalized WS_2-NPs showed a peak at ~ 449 cm^{-1} **(Fig. 3.IAa i region)** that is a characteristic frequency of tungsten disulfide [45], which confirmed the presence of inorganic support for enzyme immobilization. FTIR spectral peaks located at ~ 1635 cm^{-1} and ~ 3441 cm^{-1} revealed the presence of $–NH_2$ and –OH functional groups [46] on the surface of WS_2-NPs. These results confirmed the presence of oxygen and amino containing functional groups at the surface of the functionalized WS_2-NPs as shown in **Fig. 3.IAa.**

Thereafter, the functionalized WS_2-NPs were activated with glutaraldehyde, in which –CHO group of one arm bound to $–NH_2$ group of WS_2-NPs whereas –CHO group of the other arm remained free [19], which were confirmed by the peaks obtained at ~ 1658 cm^{-1} and ~ 1709 cm^{-1}, respectively **(Fig. 3.IAb ii region)**. The free –CHO group of the glutaraldehyde bonded to the enzyme via –NH2 group of lysine, which was confirmed by the peak obtained at ~ 1683 cm^{-1} for

–C=N. Finally, peaks located at ~ 1628 cm^{-1}, ~ 1635 cm^{-1} for Amide I and ~ 1458 cm^{-1} , ~ 1464 cm^{-1} for Amide II [47, 48] revealed that the enzyme has been immobilized successfully onto WS_2-NPs via glutaraldehyde linkage (**Fig. 3.IAc iii region)**.

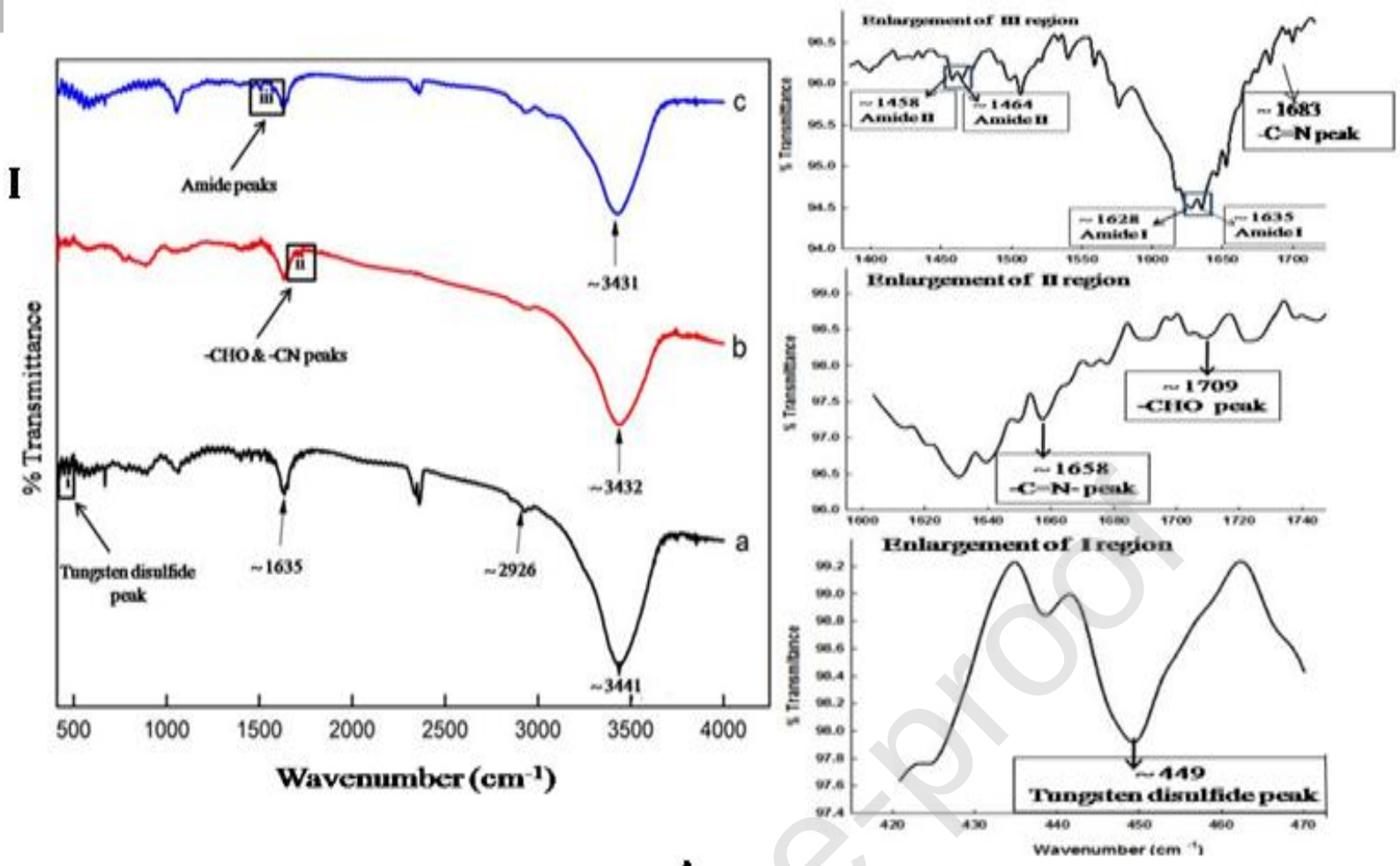

A

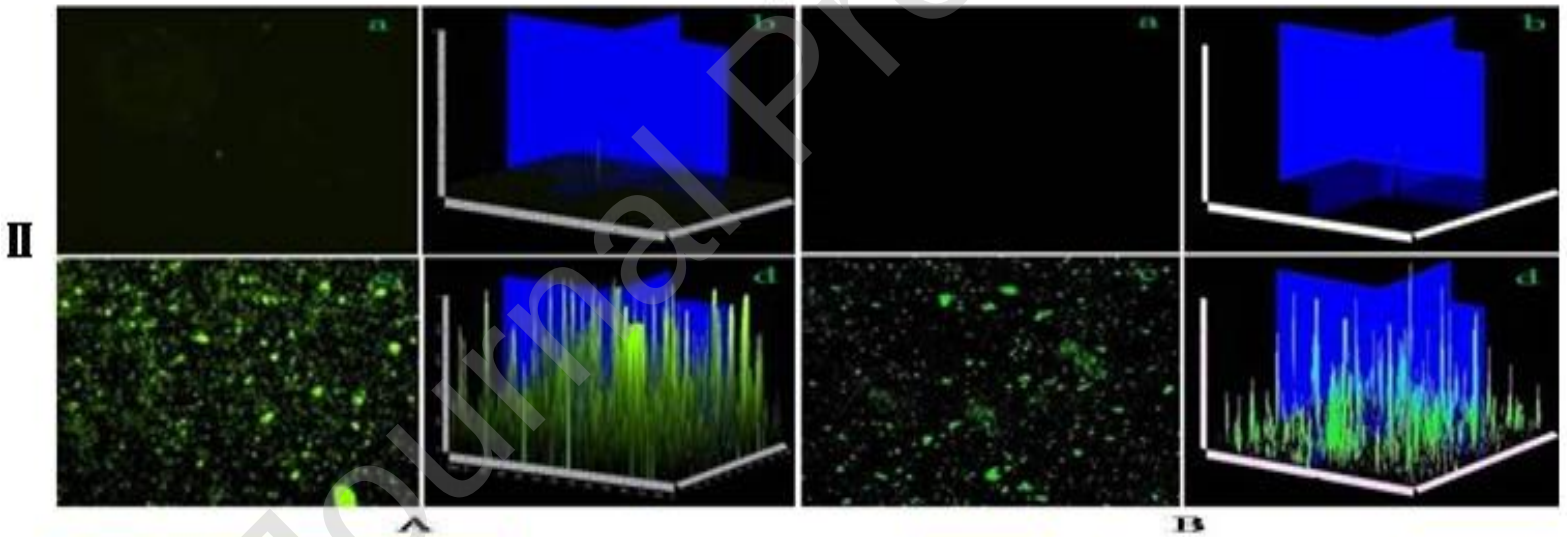

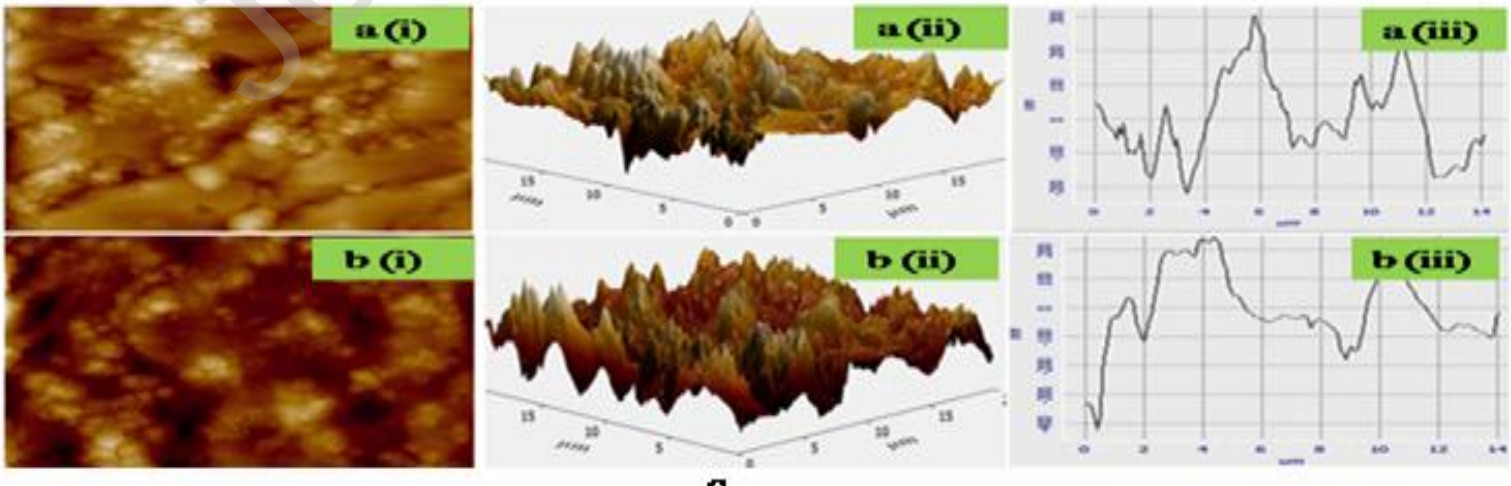

C

Fig. 3. Characterization of immobilizattungion using **(1.A)** FTIR **(a)** Native WS_2-NPs **(b)** Glutaraldehyde activated WS_2-NPs **(c)** Enzyme-linked glutaraldehyde activated WS_2-NPs. (**II.A)** Fluorescence microscopy **(a)** Native 2-D **(b)** Native 3-D image **(c)** Enzyme-linked 2-D image **(d)** Enzyme-linked 3-D image **(II.B)** Confocal microscopy image **(a)** Native 2-D **(b)** Native 3-D image **(c)** Enzyme linked 2-D **(d)** Enzyme linked 3-D image **(II.C)** AFM **(a)** Glutaraldehyde activated WS_2-NPs **(i)** 2-D **(ii)** 3-D image and **(iii)** Corresponding roughness height profile **(b)** Enzyme linked glutaraldehyde activated WS_2-NPs **(i)** 2-D **(ii)** 3-D image and **(iii)** Corresponding roughness height profile.

Fluorescence and Laser Scanning Confocal Microscopy

To further validate the results, fluorescence **(Fig. 3.IIA)** and laser confocal scanning **(Fig. 3.IIB)** microscopy were performed for native as well as immobilized enzyme. In case of immobilized enzyme a heterogeneous distribution of fluorescence (**Fig. 3.IIAc and Fig. 3.IIBc**) and fluorescence intensity peaks ((**Fig. 3.IIAd and Fig. 3.IIBd**) were observed whereas no fluorescence (**Fig. 3.IIAa and Fig. 3.IIBa**) and fluorescence intensity peaks (**Fig. 3.IIAb and Fig. 3.IIBb**) were detected in native WS_2-NPs, which revealed that the enzyme has been immobilized successfully on the matrix and presence of aggregation (**Fig. 3.IIAc and Fig. 3.IIBc**) revealed heterogeneous attachment of the enzyme onto WS_2-NPs. Similar results were reported recently for peanut β-amylase [19].

Atomic Force Microscope

AFM was used to qualitative and quantitative analysis of glutaraldehyde activated and enzyme-linked glutaraldehyde activated WS_2-NPs. AFM images of enzyme-linked glutaraldehyde activated WS_2-NPs **[Fig. 3.IICb(i) and Fig. 3.IICb(ii)]** showed different surface topography with respect to glutaraldehyde activated WS_2-NPs **[Fig. 3.IICa(i) and Fig. 3.IICa(ii)]**, which exhibited that the enzyme has been immobilized on WS_2-NPs. Moreover, roughness profiles depicted that the maximum height in case of enzyme-linked WS_2-NPs was greater (0.662 μm) than that of enzyme free WS_2-NPs (0.484 μm) as shown in **Fig. 3.IICb(iii) and Fig. 3.IICa(iii),** respectively which confirmed that the enzyme has been immobilized successfully on WS_2-NPs. An increased average roughness and root mean square roughness after immobilization further

supported the results that the enzyme has been immobilized successfully on the surface [49] of WS_2-NPs via glutaraldehyde.

Steady state kinetics

Most of the disorders and diseases are due to alteration in the 3-D conformation as well as activity of an enzyme under different environmental conditions. Therefore, understanding of enzyme activity under different condition such as change in pH, temperature and different concentration of metabolites becomes an important criterion of enzymologists Moreover, industrial point of views, it is important to know about the storage and thermal stability of an enzyme to decrease the cost of an industrial product. Therefore, study of steady state kinetics of an enzyme becomes an important criterion for enzymologists.

Effect of pH

The optimum pH of free and immobilized *β*-amylase was found to be 5.7 and 6.5, respectively. **Fig. 4a** depicts that immobilized enzyme showed higher stability in the pH range of 5.0-10.0 and retained more than 75% of relative activity at pH 10.0, which revealed less sensitivity of the immobilized *β*-amylase with respect to pH changes. Fenugreek *β*-Amylase immobilized on chitosan coated PVC beads also showed similar results [44] whereas in case of peanut *β*-amylase no change in optimum pH was observed [19]. The shift in pH optimum was due to the alteration in the ionization state of the amino acids present in the enzyme and functional groups present on the matrix whereas operational broader pH range was resulting from multipoint attachment of the enzyme to the matrix, which prevent the enzyme to be denatured upon pH alteration [50].

Effect of temperature

The optimum temperature for immobilized enzyme was 60 ºC whereas for soluble enzyme it was 57 ºC (**Fig 4b).** Fenugreek *β*-amylase immobilized on functionalized WS_2-NPs retained 82% of residual activity at 70 ºC while the soluble enzyme lost around 92% activity at the same temperature. Thus, an increase in optimum temperature is an indication of conformational rigidity, which makes the enzyme more resistant to high temperature [10].

Effect of substrate concentration

The value of K_m (5.49 mg/mL) was higher whereas V_{max} (666.67 μmoles/min/mg) was lower compared to the soluble enzyme **(Fig. 4c)**, which revealed decrease in affinity (toward substrate) and catalytic efficiency of the enzyme after immobilization (**Table S.1 given in supplementary material**). Similar results have been reported by various researchers [9, 19, 51]. These changes in K_m and V_{max} may be due to conformational changes in the enzyme's structure, introduced by immobilization process, which limit the accessibility of the substrate to its active site [52].

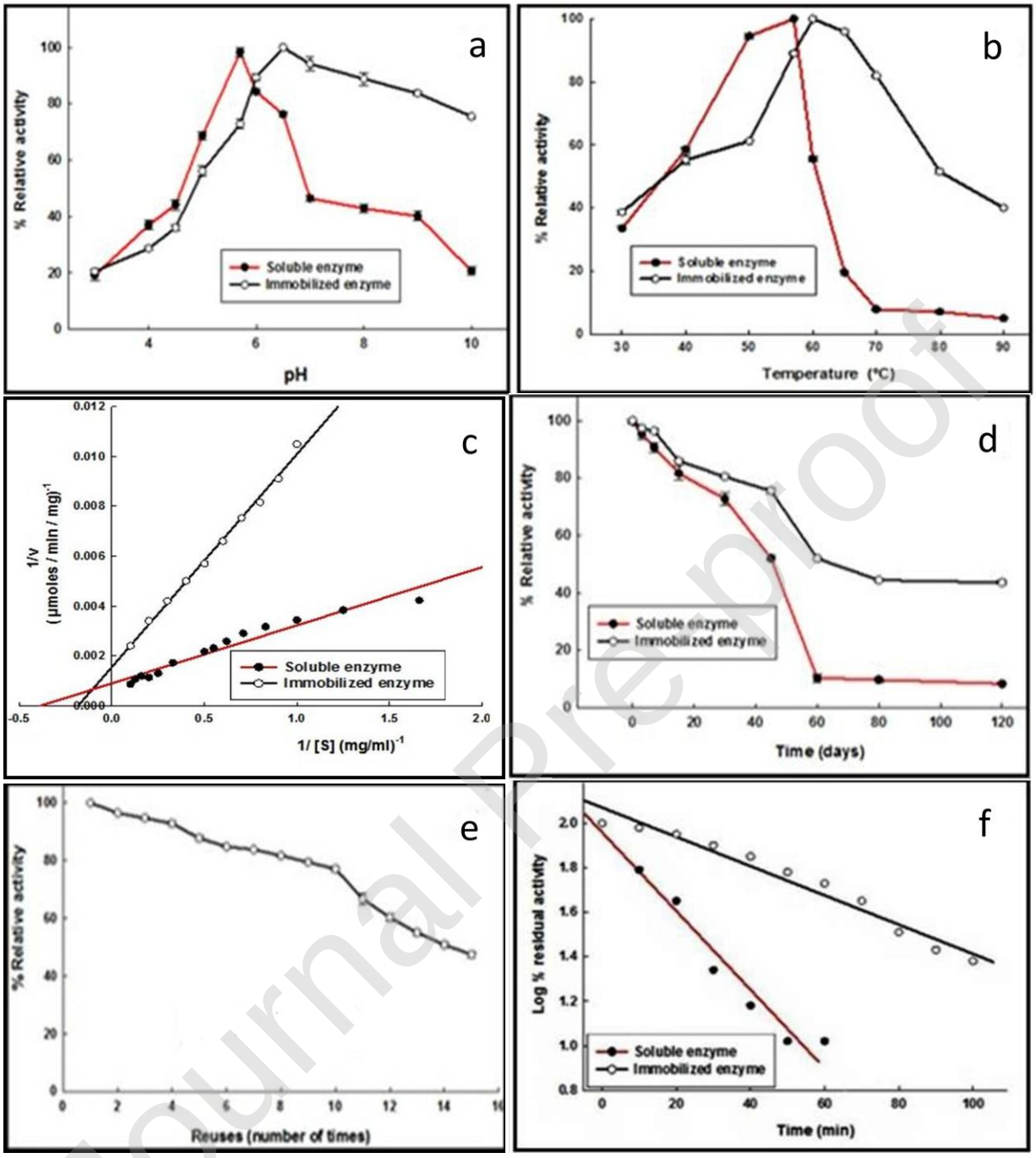

Fig. 4: Kinetics of soluble and immobilized fenugreek *β*-amylase. Effect of **(a)** pH **(b)** temperature **(c)** substrate concentration **(d)** Storage stability **(e)** Reusability and **(f)** Thermal denaturation studies.

Storage stability

Storage stability is an important parameter, which decides industrial applicability and process economy for commercialization of an enzyme. Storage stability can be enhanced by immobilizing an enzyme on a suitable matrix, which reduces the rate of enzyme denaturation [52]. **Fig. 4d** revealed that immobilized enzyme retained around 40% residual activity after 120 days at 4 °C, while soluble enzyme lost more than 90% activity under the similar conditions. These results revealed that immobilization of enzyme via glutaraldehyde provide multipoint attachment of the enzyme to the matrix, which reduced the rate of enzyme denaturation [10] and thereby increased the storage stability of the enzyme.

Reusability

Industrial applicability of an enzyme is determined by process economy that is why reusability of an enzyme becomes an important criterion for enzyme production. Reusability is the characteristic of immobilized enzyme, which allows easy removal and reuse of the enzyme after a reaction. **Fig. 4e** depicts that β-amylase immobilized onto WS_2-NPs retained around 77% and 47% relative activity after 10 and 15 uses, respectively whereas in case of β-amylase immobilized onto functionalized graphene sheets, it was 76% after 10 uses [10]. The loss in an enzyme activity could be due to leakage of immobilized enzyme from a matrix because of the weakness of binding strength between the immobilized enzyme and the matrix occurring due to the repeated use of the immobilized enzyme [53].

Thermal stability study

Stability of enzyme at higher temperature, decreases viscosity of the medium, increases rate of reaction, decreases operational time and thereby decreases the cost of biological process. That is why, study of thermal stability becomes a crucial factor for the use of an enzyme for industrial applications [54, 55]. Multiple correlation coefficients, kinetic rate constant (k) and half life were determined according to the procedure and expression given in material and methods. Multiple correlation coefficient was found to be greater than 93% that revealed thermal inactivation study followed first-order kinetics The half life of immobilized enzyme was higher (lower kinetic rate constant) compare to soluble enzyme at same temperature **(Table S.2 given in supplementary**

material), which revealed increased in thermal stability after immobilization. For instance, at 60 °C (**Fig. 4e**) for immobilized enzymes, $t_{1/2}$ was found to be 49 min (k 0.0202 min^{-1}) whereas in case of soluble enzyme it was 11 min (k 0.0941 min^{-1}).

These results revealed increased in thermal stability after immobilization, which might be due to multipoint attachment of the enzyme to functionalized WS_2-NPs via glutaraldehyde that protect the amide linkage of the enzyme from disruption, leading to increase in enzyme stability at higher temperature [56].

Interaction of sugars with *β*-amylase

Among three aromatic amino acids present in a protein, tryptophan (Trp) has the highest quantum yield and gives good fluorescence signals. Because of this unique property, change in fluorescent intensity of tryptophan was used as a probe to study the conformational changes, which occur upon the interaction of ligand with Trp residues present in protein molecules [57]. Under our experimental conditions, fluorescence signals from maltose, sucrose, buffer and matrix were so weak that the influence of these parameters may be neglected safely. The fluorescence peaks obtained around 340 nm revealed the presence of interior tryptophan residues in the fenugreek *β*-amylase [58, 59]. **Fig. 5Aa** and **Fig. 5Ba** show that there was a gradual decrease in the fluorescence intensity of fenugreek *β*-amylase with respect to increasing concentrations of maltose and sucrose, respectively. The changes in the microenvironment (due to addition of ligands) around tryptophan lead to change in the 3D conformation of an enzyme, which might cause the unfolding of the enzyme resulting in the exposure of buried tryptophan residues present in the enzyme. These exposed tryptophan residues are quenched by increasing concentration of ligand (sucrose or maltose) and thereby decrease in quantum yield of tryptophan was observed [60].

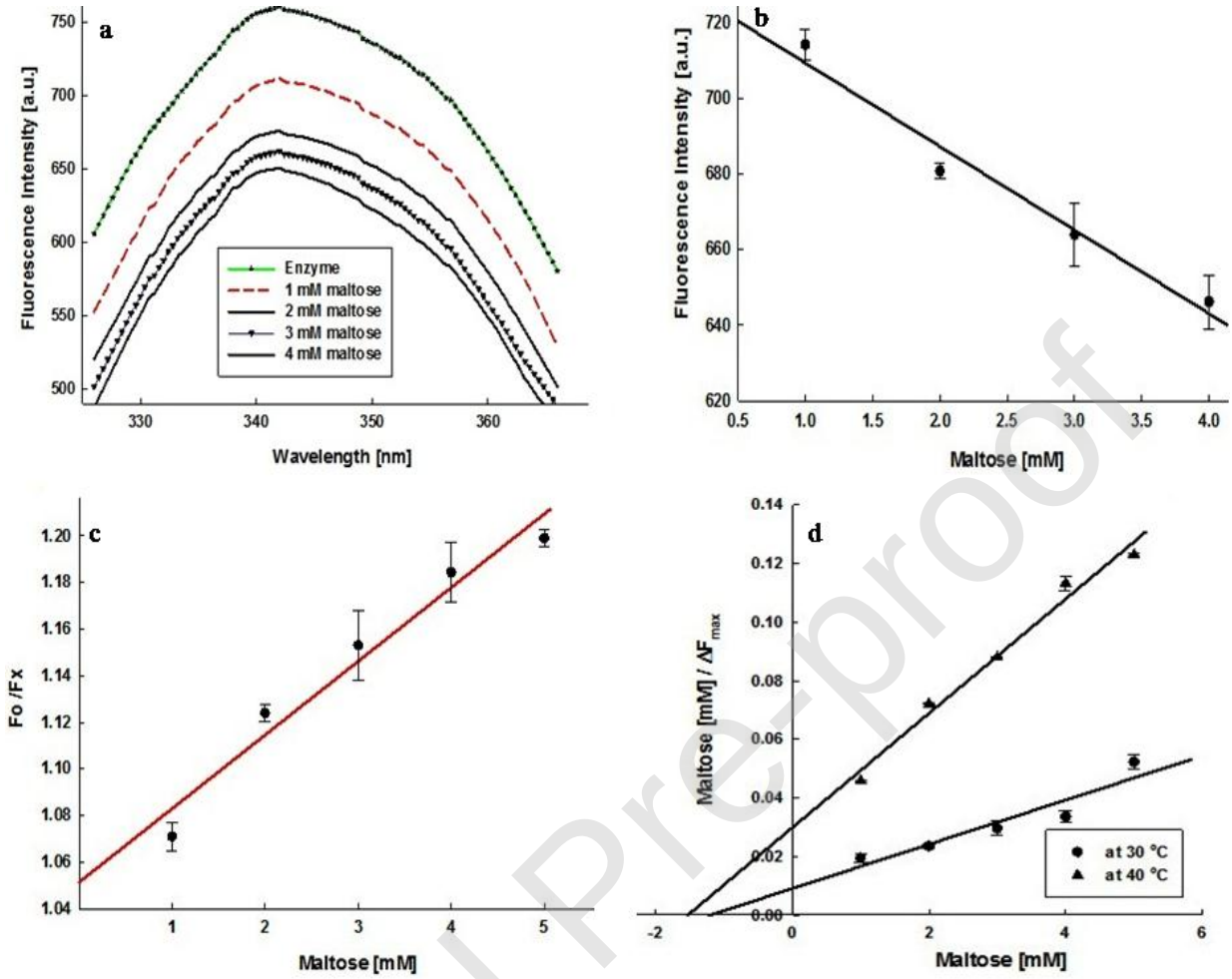

(A)

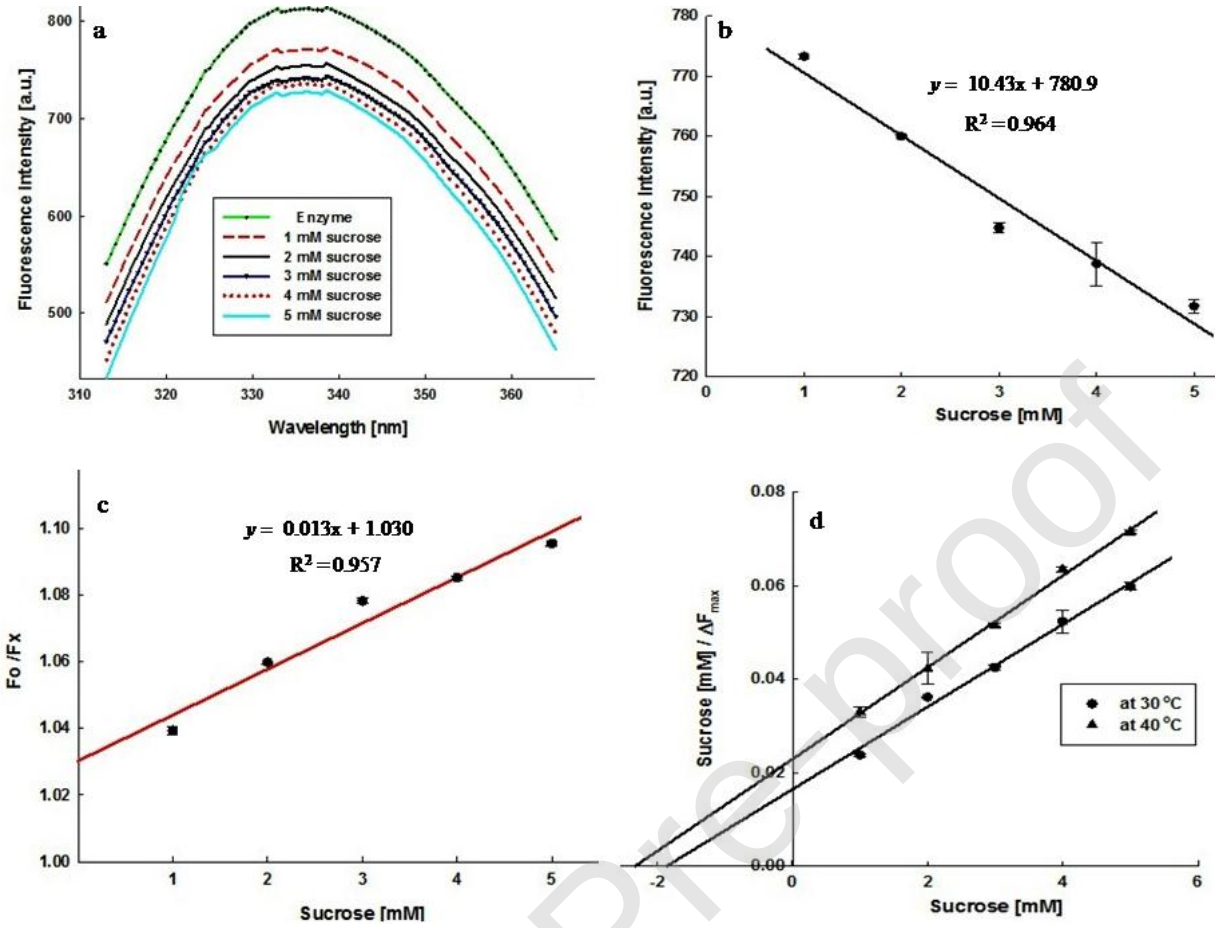

(B)

Fig. 5: Interaction of *β*-amylase with **(A) maltose (a)** Quenching of trp fluorescence intensity **(b)** Relationship between maximum fluorescence intensity with respect to maltose concentration **(c)** Stern-Volmer plot **(d)** Hanes-Woolf plot to determine dissociation constant. (**B) Sucrose (a)** Quenching of trp fluorescence intensity **(b)** Linear relationship between fluorescence intensity with respect to sucrose to find out limit of detection **(c)** Stern-Volmer plot **(d)** Hanes-Woolf plot to determine dissociation constant.

Quenching and Stern-Volmer graphs for maltose **(Fig. 5Ab and Fig. 5Ac)** and sucrose **(Fig. 5Bb and Fig. 5Bc)** were plotted. Multiple correlation coefficient R^2 values obtained from quenching (0.97) and Stern-Volmer (0.96) plots revealed linear relationship between fluorescence quenching and concentration of ligand in the range of 1-4 mM and 1-5 mM for maltose and sucrose, respectively. Limit of detection values were found to be 0.052 mM and 0.096 mM for maltose and sucrose, respectively. In case of amperometric sucrose biosensor the linearity was

up to 5 mM, which was similar to our results whereas limit of detection was found to be 0.002 mM [61]. The dissociation constant is the concentration of ligand, at which 50% binding sites of a biomolecule are occupied. It shows the affinity between ligand and biomolecule. Affinity constant (K_a) is inverse of the dissociation constant and could be calculated using K_d values ($K_d = 1/K_a$). Hanes-Woolf plots are shown in **Fig. 5Ad** and **Fig. 5Bd** for maltose and sucrose, respectively and results are shown in **Table 3A**, which revealed higher affinity of maltose with the enzyme. Importantly, it was also observed that the value of the dissociation constant increases as the temperature increased as shown in **Table 3A** [62]. Dissociation constants calculated from Hanes-Woolf plot were used for calculating thermodynamic parameters such as changes in enthalpy (ΔH), entropy (ΔS) and Gibbs free energy (ΔG) using the equations 3,4 and 5 described in the above section and results are presented in **Table 3A**. Thermodynamic parameter ΔG was found to be negative that showed spontaneous nature of the reaction whereas positive values of ΔH revealed endothermic nature of the interaction. The interaction between biological macromolecule and ligand belongs to mainly weak forces such as van der Waals force, hydrogen bonding, electrostatic and hydrophobic interaction [63] and could be evaluated using thermodynamic parameters using the criteria as given in **Table 3B**. The positive values of ΔS and ΔH revealed that the interaction between sugar molecule and *β*-amylase is driven by hydrophobic interactions.

Table 3 (A): Thermodynamic parameters of interaction of fenugreek *β*-amylase with sugars

Ligand	Temperature (^{0}C)	K_d (mM)	K_a (mM^{-1})	ΔG (kJ/mole)	ΔH (kJ/mole)	TΔS (kJ/mole)
Sucrose	30	2.00	0.50	-1.745	15.733	17.478
	40	2.44	0.41	-2.330		18.053
Maltose	30	1.28	0.78	-0.632	16.255	16.888
	40	1.58	0.63	-1.187		17.443

(B): Criteria for deciding kind of interaction involved between ligand and biomolecules

Interaction	Condition
Hydrophobic	ΔH > 0 and Δ S > 0
Hydrogen Bonding	ΔH < 0 and Δ S < 0
Electrostatic	ΔH < 0 and Δ S > 0

Conclusions

In this paper fenugreek *β*-amylase was immobilized onto WS_2-NPs using glutaraldehyde as a cross-linker. To confirm the binding of the enzyme onto WS_2-NPs, SEM, AFM, FT-IR, fluorescence and confocal microscopy were employed. A statistical program, Box-bhenkan design of RSM was used to optimize process parameters. After optimization predicted (85.58%) and actual (84.21%) immobilization efficiency were very close, which revealed the successfulness of the model. The immobilized enzyme showed greater storage and higher thermal stability compared to the soluble enzyme. Dissociation constant for maltose was found to be lower than sucrose, which revealed higher affinity of maltose with the enzyme. Positive values of thermodynamic parameter such as changes in enthalpy ($\Delta H > 0$) and entropy ($\Delta S > 0$) revealed that the process is endothermic that is driven by the hydrophobic interactions. Change in Gibbs free energy ($\Delta G < 0$) revealed that the process is spontaneous in nature. Fluorescence quenching followed first-order kinetics with limit of detection 0.052 and 0.096 mM for maltose and sucrose, respectively. This is the first attempt to develop fluorescence biosensor based on quenching of tryptophan residues present in the *β*-amylase to detect maltose and sucrose in food and beverage industries. This work can be extended to detect metal ions in a sample to control environmental metal toxicity.

Acknowledgments

Dinesh C. Agrawal would like to thank the University Grants Commission (UGC), New Delhi, India for financial support in the form of Junior and Senior Research Fellowships (Ref. no. 23-06/2013 (i) EU-V). V.K.S. acknowledges the UGC for providing Senior Research Fellowship (Fellowship Grant No: F.25-1/2014-15/(BSR)/5-127/2007/(BSR). A.S. acknowledges DST-PURSE, SERB, India (Project Code: EMR/2016/007720) and CAS-BHU for providing financial support. Arvind M. Kayastha is thankful for financial grant supported by University Potential for Excellence (UGC-UPE) from Banaras Hindu University. We acknowledge Central

Instrumentation Facility (CIF) and Interdisciplinary School of Life Sciences (ISLS) at Banaras Hindu University for use of several sophisticated equipments, required for data collection.

Conflict of interest

Authors declare no competing financial interest.

Appendix A. Supplementary data

Supplementary data (Table S.1, Table S.2 and Fig. S) are attached as doc file to this article:

References

[1]. Scheidig A, Fröhlich A, Schulze S, Lloyd JR, Kossmann J. Downregulation of a chloroplast-targeted *β*-amylase leads to a starch-excess phenotype in leaves. Plant J, 2002; 30(5): 581-591.

[2]. Baba T, Kainuma K. Partial hydrolysis of sweet-potato starch with *β*-amylase. Agri Biol Chem, 1987; 51(5): 1365-1371.

[3]. Srivastava G, Kayastha AM. *β*-Amylase from starchless seeds of *Trigonella foenum-graecum* and its localization in germinating seeds. PloS One, 2014; 9(2): e88697.

[4]. Pyeshkova V, Saiapina O, Soldatkin O, Dzyadevych S. Enzyme conductometric biosensor for maltose determination. Biopolym Cell, 2009; 25(4): 272-278.

[5]. Jacob R, Zimmer KP, Schmitz J, Naim HY. Congenital sucrase-isomaltase deficiency arising from cleavage and secretion of a mutant form of the enzyme. J Clin Invest, 2000; 106(2): 281-287.

[6]. Olaiya OE, Kolawole AN, Kolwole A. Interaction of metronidazole with aldehyde dehydrogenase: spectroscopic approach. Rom J Biophys, 2016; 26(4).

[7]. Hu Y, Da L. Insights into the selective binding and toxic mechanism of microcystin to catalase. Spectrochimica Acta A: Mol Biomol Spectrosc, 2014; 121: 230-237.

[8]. Pasban Ziyarat F, Asoodeh A, Sharif Barfeh Z, Pirouzi M, Chamani J. Probing the interaction of lysozyme with ciprofloxacin in the presence of different-sized Ag nano-particles

by multispectroscopic techniques and isothermal titration calorimetry. J Biomol Struct Dyn, 2014; 32(4): 613-629.

[9]. Das R, Talat M, Srivastava O, Kayastha AM. Covalent immobilization of peanut β-amylase for producing industrial nano-biocatalysts: A comparative study of kinetics, stability and reusability of the immobilized enzyme. Food Chem, 2018; 245: 488-499.

[10]. Singh K, Srivastava G, Talat M, Srivastava ON, Kayastha AM. α-Amylase immobilization onto functionalized graphene nanosheets as scaffolds: Its characterization, kinetics and potential applications in starch based industries. Biochem Biophys Rep, 2015; 3: 18-25.

[11]. Hanefeld U, Gardossi L, Magner E. Understanding enzyme immobilisation. Chem Soc Rev, 2009; 38(2): 453-468.

[12]. Sheldon RA, Pelt SV. Enzyme immobilisation in biocatalysis: why, what and how? Chem Soc Rev, 2013; 42: 6223-6235.

[13]. Joshi KA, Tang J, Haddon R, Wang J, Chen W, Mulchandani A. A disposable biosensor for organophosphorus nerve agents based on carbon nanotubes modified thick film strip electrode. Electroanalysis, 2005; 17(1): 54-58.

[14]. Joshi KA, Prouza M, Kum M, Wang J, Tang J, Haddon R, Chen W, Mulchandani A. V-type nerve agent detection using a carbon nanotube-based amperometric enzyme electrode. Anal Chem, 2006; 78(1): 331-336.

[15]. Chiang CJ, Hsiau LT, Lee WC. Immobilization of cell-associated enzymes by entrapment in polymethacrylamide beads. Biotechnol Tech, 1997; 11(2): 121-125.

[16]. Klotzbach TL, Watt M, Ansari Y, Minteer SD. Improving the microenvironment for enzyme immobilization at electrodes by hydrophobically modifying chitosan and Nafion® polymers. J Memb Sci, 2008; 311(1-2): 81-88.

[17]. Roy I, Sardar M, Gupta MN. Cross-linked alginate-guar gum beads as fluidized bed affinity media for purification of jacalin. Biochem Eng J, 2005; 23(3): 193-198.

[18]. Sardar M, Gupta MN. Immobilization of tomato pectinase on Con A-Seralose 4B by bioaffinity layering. Enzyme Microb Technol, 2005; 37(3): 355-359.

[19]. Das R, Mishra H, Srivastava A, Kayastha AM. Covalent immobilization of β-amylase onto functionalized molybdenum sulfide nanosheets, its kinetics and stability studies: A gateway to boost enzyme application. Chem Eng J, 2017; 328: 215-227.

[20]. Hosseini SH, Hosseini SA, Zohreh N, Yaghoubi M, Pourjavadi A. Covalent immobilization of cellulase using magnetic poly (ionic liquid) support: improvement of the enzyme activity and stability. J Agri Food Chem, 2018; 66(4): 789-798.

[21]. Mateo C, Palomo JM, Fernandez-Lorente G, Guisan JM, Fernandez-Lafuente R. Improvement of enzyme activity, stability and selectivity via immobilization techniques. Enzyme Microb Technol, 2007; 40(6): 1451-1463.

[22]. Patila M, Kouloumpis A, Gournis D, Rudolf P, Stamatis H. Laccase-functionalized graphene oxide assemblies as efficient nanobiocatalysts for oxidation reactions. Sensors, 2016; 16(3): 287-301.

[23]. Pavlidis I, Patila M, Bornscheuer U, Gournis D, Stamatis H. Graphene-based nanobiocatalytic systems: recent advances and future prospects. Trends Biotechnol, 2014; 32(6): 312-320.

[24]. Marcano DC, Kosynkin DV, Berlin JM, Sinitskii A, Sun Z, Slesarev A, Alemany LB, Lu W, Tour JM. Improved synthesis of graphene oxide. ACS Nano, 2010; 4(8): 4806-4814.

[25]. Manzeli S, Ovchinnikov D, Pasquier D, Yazyev OV, Kis A. 2D transition metal dichalcogenides. Nat Rev Mater, 2017; 2(8): 17033.

[26]. Schutte W, De Boer J, Jellinek F. Crystal structures of tungsten disulfide and diselenide. J Solid State Chem, 1987; 70(2): 207-209.

[27]. Dwevedi A, Singh AK, Singh DP, Srivastava ON, Kayastha AM. Lactose nano-probe optimized using response surface methodology. Biosens Bioelectron, 2009; 25(4): 784-790.

[28]. Wani TA, Ahmad A, Zargar S, Khalil NY, Darwish IA. Use of response surface methodology for development of new microwell-based spectrophotometric method for determination of atrovastatin calcium in tablets. Chem Cent J, 2012; 6(1): 134-142.

[29]. Agrawal DC, Dwevedi A, Kayastha AM. Biochemical and thermodynamic characterization of de novo synthesized β-amylase from fenugreek. Int J Biol. Macromol, 2019; 130: 786-797.

[30]. Singh VK, Tiwari R, Srivastava A. Growth of Highly Crystalline Bundles of WO3 Nanorod under Facile Hydrothermal Condition. Int J Mater Sci, 2017; 12(1): 108-111.

[31]. Oosta GM, Mathewson NS, Catravas GN. Optimization of Folin-Ciocalteu reagent concentration in an automated Lowry protein assay. Anal Biochem, 1978; 89(1): 31-34.

[32]. Bernfeld P. Amylases, alpha and beta. Methods in Enzymology,1955; 1: 149-158.

[33]. Córdova FC, León AG, Reyes RG, González MG, Regalado ES, González MS, Lopez IQ. Response surface methodology for lead biosorption on *Aspergillus terreus*. Int J Environ Sci Technol, 2011; 8(4): 695-704.

[34]. Noordin MY, Venkatesh VC, Sharif S, Elting S, Abdullah A. Application of response surface methodology in describing the performance of coated carbide tools when turning AISI 1045 steel. J Mater Process Technol, 2004; 145(1): 46-58.

[35]. Gangadharan D, Sivaramakrishnan S, Nampoothiri KM, Sukumaran RK, Pandey A. Response surface methodology for the optimization of alpha amylase production by *Bacillus amyloliquefaciens*. Bioresour Technol, 2008; 99(11): 4597-4602.

[36]. Srivastava G, Singh K, Talat M, Srivastava ON, Kayastha AM. Functionalized graphene sheets as immobilization matrix for fenugreek *β*-amylase: enzyme kinetics and stability studies. PloS One, 2014; 9(11): e113408.

[37]. Marcuello C, De Miguel R, Gómez-Moreno C, Martinez-Julvez M, Lostao A. An efficient method for enzyme immobilization evidenced by atomic force microscopy. Protein Eng Des Sel, 2012; 25(11): 715-723.

[38.] Pal A, Lobo M, Khanum F. Extraction, purification and thermodynamic characterization of almond (*Amygdalus communis) β*-galactosidase for the preparation of delactosed milk. Food Technol Biotechnol, 2013, 51(1): 53-61.

[39]. Ohnishi M, Yamashlta T, Hiromp K. Static and kinetic studies by fluorometry on the interaction between gluconolactone and glucoamylase from *Rh. niveus*. J Biochem, 1977; 81(1): 99-105.

[40]. Horn JR, Russell D, Lewis EA, Murphy KP. Van't Hoff and calorimetric enthalpies from isothermal titration calorimetry: are there significant discrepancies? Biochemistry, 2001; 40(6): 1774-1778.

[41]. Rao SV, Anderson KW, Bachas LG. Oriented immobilization of proteins. Microchim Acta.,1998; 128(3-4): 127-143.

[42]. Karam EA, Wahab WAA, Saleh SA, Hassan ME, Kansoh AL, Esawy MA. Production, immobilization and thermodynamic studies of free and immobilized *Aspergillus awamori* amylase. Int J Biol Macromol, 2017; 102: 694-703.

[43]. Saleem M, Rashid M, Jabbar A, Perveen R, Khalid A, Rajoka M. Kinetic and thermodynamic properties of an immobilized endoglucanase from *Arachniotus citrinus*. Process Biochem, 2005; 40(2): 849-855.

[44]. Srivastava G, Roy S, Kayastha AM. Immobilisation of fenugreek *β*-amylase on chitosan/PVP blend and chitosan coated PVC beads: A comparative study. Food Chem, 2015; 172: 844-851.

[45]. Zhao X, He D, Wang Y, Fu C. Facile fabrication of tungsten disulfide quantum dots (WS_2 QDs) as effective probes for fluorescence detection of dopamine (DA). Mater Chem Phys, 2018; 207: 130-134.

[46]. Ramanathan T, Fisher F, Ruoff R, Brinson L. Amino-functionalized carbon nanotubes for binding to polymers and biological systems. Chem Mater, 2005; 17(6): 1290-1295.

[47]. Secundo F. Conformational changes of enzymes upon immobilisation. Chem Soc Rev, 2013; 42(15): 6250-61.

[48]. Barth A. Infrared spectroscopy of proteins. Biochim Biophys Acta Bioenerg, 2007; 1767(9): 1073-1101.

[49]. Zhang P, Tan W. Atomic force microscopy for the characterization of immobilized enzyme molecules on biosensor surfaces. Fresenius J Anal Chem, 2001; 369(3-4): 302-307.

[50]. Singh K, Kayastha AM. Optimal immobilization of *α*-amylase from wheat (*Triticum aestivum*) onto DEAE-cellulose using response surface methodology and its characterization. J Mol Catal B: Enzym, 2014; 104: 75-81.

[51]. Tavano OL, Fernandez-Lafuente R, Goulart AJ, Monti R. Optimization of the immobilization of sweet potato amylase using glutaraldehyde-agarose support: Characterization of the immobilized enzyme. Process Biochem, 2013; 48(7): 1054-1058.

[52]. A Chaudhari S, R Kar J, S Singhal R. Immobilization of proteins in alginate: functional properties and applications. Curr Org Chem, 2015; 19(17): 1732-1754.

[53]. Danial EN, Hamza AH, Mahmoud RH. Characteristics of immobilized urease on grafted alginate bead systems. Braz Arch Biol Technol, 2015; 58(2): 147-153.

[54]. Zamost BL, Nielsen HK, Starnes RL. Thermostable enzymes for industrial applications. J Ind Microbiol, 1991; 8(2): 71-81.

[55]. Littlechild JA. Enzymes from extreme environments and their industrial applications. Front Bioeng Biotechnol, 2015; 3: 161-169.

[56]. Mohapatra SC, Hsu JT. Time dependent behaviour of the cross-linking reaction of α-chymotrypsin with glutaraldehyde. Biotechnol Techn, 1994; 8(1): 13-16.

[57]. Chen Y, Barkley MD. Toward understanding tryptophan fluorescence in proteins. Biochemistry, 1998; 37(28): 9976-9982.

[58]. Burstein E, Vedenkina N, Ivkova M. Fluorescence and the location of tryptophan residues in protein molecules. Photochem Photobiol, 1973; 18(4): 263-279.

[59]. Fujiwara K, Inouye K, Tonomura BI, Murao S, Tsuru D. Interaction of thiol subtilisin with *Streptomyces* subtilisin inhibitor, SSI. J Biochem, 1977; 82(1): 125-130.

[60]. Yang MM, Xiao Q, Xi XL. Study of the interaction of cephalosporin class medicine with albumin by fluorescence enhancement and fluorescence quenching theories. Chin J Chem, 2006; 24(5): 642-648.

[61]. Antiochia R, Gorton L, Mannina L. Rapid Determination of Sucrose in Fruit Juices: A New Sensitive Carbon Nanotube Paste Osmium-Polymer Mediated Biosensor. J Food Res Biopolym Cell. 2014; 3(4): 101-112.

[62]. Kitagishi K, Hiromi K, Oda K, Murao S. Equilibrium study on the binding between thermolysin and *Streptomyces* metalloprotease inhibitor, talopeptin (MKI). J Biochem, 1983; 93(1): 47-53.

[63]. Ross PD, Subramanian S. Thermodynamics of protein association reactions: forces contributing to stability. Biochemistry, 1981; 20(11): 3096-3102.